Redox Biology 49 (2022) 102224

Contents lists available at ScienceDirect

Redox Biology

journal homepage: www.elsevier.com/locate/redox

Inhibition of GCN2 alleviates hepatic steatosis and oxidative stress in obese mice: Involvement of NRF2 regulation

Juntao Yuan, Zhuoran Yu, Junling Gao, Kai Luo, Xiyue Shen, Bingqing Cui, Zhongbing Lu *

College of Life Science, University of Chinese Academy of Sciences, Beijing, 100049, China

ARTICLE INFO

Keywords:
GCN2
NRF2
KEAP1
Hepatic steatosis
Oxidative stress

ABSTRACT

The development of nonalcoholic fatty liver disease (NAFLD) is associated with increased reactive oxygen species (ROS) production. Previous observations on the contradictory roles of general control nonderepressible 2 (GCN2) in regulating the hepatic redox state under different nutritional conditions prompted an investigation of the underlying mechanism by which GCN2 regulates ROS homeostasis. In the present study, GCN2 was found to interact with NRF2 and decrease NRF2 expression in a KEAP1-dependent manner. Activation of GCN2 by halofuginone treatment or leucine deprivation decreased NRF2 expression in hepatocytes by increasing GSK-3β activity. In response to oxidative stress, GCN2 repressed NRF2 transcriptional activity. Knockdown of hepatic GCN2 by tail vein injection of an AAV8-sh*Gcn2* vector attenuated hepatic steatosis and oxidative stress in leptin-deficient (ob/ob) mice in an NRF2-dependent manner. Inhibition of GCN2 by GCN2iB also ameliorated hepatic steatosis and oxidative stress in both ob/ob mice and high fat diet-fed mice, which was associated with significant changes in lipid and amino acid metabolic pathways. Untargeted metabolomics analysis revealed that GCN2iB decreased fatty acid and sphingomyelin levels but increased aliphatic amino acid and phosphatidylcholine levels in fatty livers. Collectively, our results provided the first direct evidence that GCN2 is a novel regulator of NRF2 and that specific GCN2 inhibitors might be potential drugs for NAFLD therapy.

1. Introduction

As an important metabolic organ, the liver is often impaired or even pathologically damaged by overnutrition, obesity and metabolic syndrome [1]. Lipotoxicity is one of the most frequent causes of liver abnormalities [2,3]. Moreover, the liver can also be injured by chemical toxins, viruses and pathogens [4,5]. Many of these types of disorders are associated with increased reactive oxygen species (ROS) production, and oxidative stress is one of the most important mechanisms for multiple hepatic diseases, including alcoholic or nonalcoholic fatty liver disease (NAFLD), hepatitis C virus infection, steatohepatitis and cirrhosis [1,6–8].

Nuclear factor erythroid 2-related factor 2 (NRF2) play an important role in maintaining cellular redox homeostasis. Under normal conditions, NRF2 is negatively regulated by Kelch-like ECH-associated protein 1 (KEAP1) through the connection between NRF2 and Cullin-3 (Cul3), which forms a ubiquitin E3 ligase complex [9,10]. In response to oxidants, NRF2 is released from the complex and translocates to the nucleus to form a heterodimer with the small MAF protein, which then activates the transcription of antioxidant and detoxification genes that contain antioxidant response element (ARE) sequences in their promoters [11]. NRF2 also affects hepatic lipid metabolism. Genetic deletion of *Nrf2* profoundly increases the susceptibility of mice to nonalcoholic steatohepatitis (NASH) and cirrhosis upon consumption of a high-fat diet (HFD) [12] or methionine- and choline-deficient (MCD) diet [13], whereas genetic or pharmacologic activation of NRF2 decreases their sensitivity to NASH [14,15].

As an amino acid sensor, general control nonderepressible 2 (GCN2) is activated by amino acid starvation and phosphorylates eukaryotic initiation factor 2α (eIF2α) to maintain amino acid homeostasis by attenuating global mRNA translation and inducing selective stimulation of the expression of amino acid biosynthetic genes [16,17]. GCN2 is highly expressed in the liver and is involved in the regulation of hepatic lipid metabolism and redox state under different nutritional conditions. In response to both dietary and pharmaceutical amino acid deprivation, *Gcn2*$^{-/-}$ mice display severe hepatic steatosis and increased oxidative stress [18,19]. When mice are fed a HFD, GCN2 deficiency significantly attenuates liver dysfunction, insulin resistance, hepatic steatosis and

* Corresponding author. College of Life Science, University of Chinese Academy of Sciences, 19A Yuquanlu, Beijing, 100049, China.
E-mail address: luzhongbing@ucas.ac.cn (Z. Lu).

https://doi.org/10.1016/j.redox.2021.102224
Received 6 December 2021; Accepted 21 December 2021
Available online 22 December 2021
2213-2317/© 2021 The Authors. Published by Elsevier B.V. This is an open access article under the CC BY-NC-ND license (http://creativecommons.org/licenses/by-nc-nd/4.0/).

oxidative stress in HFD-fed mice [20].

There is evidence that GCN2 may affect NRF2 pathway. For example, In high glucose-stimulated ARPE-19 cells, GCN2 depletion reduced cell apoptosis and enhanced activation of the NRF2 pathway [21]. Halofuginone (HF), a GCN2 agonist, represses NRF2 expression in NRF2-addicted cancer cells [22]. However, the mechanism by which GCN2 regulates the NRF2 pathway remains unclear. In the present study, we found that GCN2 overexpression decreased NRF2 expression via protein-protein interactions and that GCN2 activation decreased NRF2 signaling by activating glycogen synthase kinase-3β (GSK-3β). Moreover, knockdown of GCN2 improved hepatic steatosis, insulin resistance and oxidative stress in leptin-deficient (ob/ob) mice in an NRF2-dependent manner. Finally, we showed that the GCN2-specific inhibitor GCN2iB has potential therapeutic effects on NAFLD.

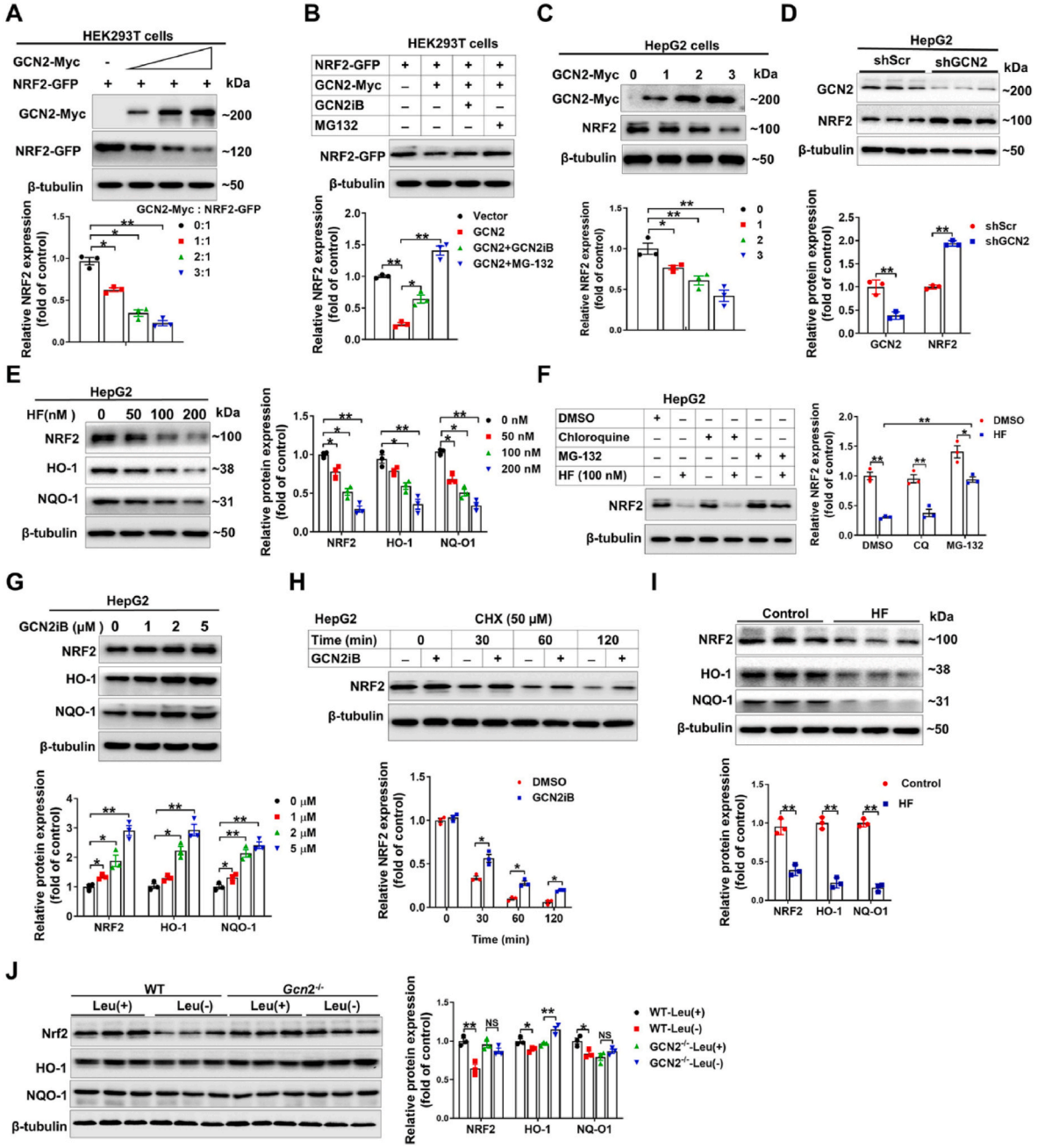

Fig. 1. GCN2 negatively regulates NRF2 expression. (A) 293T cells transfected with a NRF2-GFP expression vector and various amounts (1 × , 2 × and 3 ×) of GCN2-Myc vector were lysed and subjected to Western blot analysis with antibodies against Myc, GFP or β-tubulin (loading control). (B) 293T cells transfected with NRF2-GFP and GCN2-Myc (2 ×) vectors were treated with 2 μM GCN2iB or MG132 for 6 h and then lysed and subjected to Western blot analysis. (C) HepG2 cells were transfected with various amounts (1 × , 2 × and 3 ×) of GCN2-Myc vector for 24 h. Cells were lysed and subjected to Western blot analysis. (D) HepG2 cells were stably transfected with shRNA lentiviral vectors targeting a scrambled sequence (shScr) or GCN2 (sh*GCN2*), and cell lysates were examined by Western blot analysis. (E) HepG2 cells were treated with 0–200 nM halofuginone (HF) for 24 h, and cell lysates were then subjected to Western blot analysis. (F) HepG2 cells were cotreated with 100 nM HF and 2 μM chloroquine or MG132 for 24 h, and the cell lysates were then subjected to Western blot analysis. (G) HepG2 cells treated with 0–5 μM GCN2iB were lysed and subjected to Western blot analysis. (H) After administration of cycloheximide (CHX), control and GCN2iB-treated (2 μM) HepG2 cells were lysed at different times, and NRF2 expression in the cell lysates was determined by Western blot analysis. (I) Mice were treated with 3 mg/kg HF for 3 days, and liver lysates were examined by Western blot analysis. (J) Mice were fed a control (nutritionally complete amino acid, Leu (+)) or leucine-deficient (Leu (−)) diet for 7 days. Liver lysates were then examined by Western blot analysis. N=3, values represent the mean ± SEM; * indicates $p<0.05$; ** indicates $p<0.01$.

2. Results

GCN2 represses NRF2 expression. To investigate whether GCN2 regulates the NRF2 pathway, we transfected 293T cells with Myc epitope-tagged GCN2 (GCN2-Myc) and GFP-tagged NRF2 (NRF2-GFP) expression constructs. Forced expression of GCN2-Myc reduced the abundance of NRF2-GFP in a dose-dependent manner (Fig. 1A). The reduction in NRF2-GFP expression induced by GCN2 overexpression was significantly attenuated by treatment with 2 μM GCN2iB (a GCN2-specific inhibitor) or MG132 (a proteasome inhibitor) (Fig. 1B). In HepG2 cells, forced expression of GCN2-Myc also decreased the expression of endogenous NRF2 in a dose-dependent manner (Fig. 1C). In contrast, stable knockdown of GCN2 by transfection of a GCN2-specific shRNA lentiviral vector (shGCN2) resulted in an approximate 2-fold increase in NRF2 expression (Fig. 1D).

HF has been shown to activate GCN2 by increasing the levels of uncharged prolyl-tRNA [23]. Consistently, HF treatment increased the phosphorylation of eIF2α in HepG2 and NCTC 1469 cells (Fig. S1). Interestingly, HF decreased NRF2, heme oxygenase-1 (HO-1) and NAD(P)H quinone dehydrogenase 1 (NQO-1) expression in HepG2 and NCTC 1469 cells in a dose-dependent manner (Fig. 1E, Fig. S2). The HF-mediated decrease in NRF2 expression was attenuated by MG132, but not by chloroquine (an inhibitor of autophagy), indicating that HF decreases NRF2 expression via the proteasome pathway (Fig. 1F). In 293T cells, HF treatment significantly decreased ARE luciferase activity in control and tertiary butylhydroquinone (tBHQ)-treated 293T cells. In contrast, ARE luciferase activity was significantly increased by GCN2iB (Fig. S3).

We next treated cells with GCN2iB to examine the effect of GCN2 inhibition on NRF2 expression. In HepG2 and NCTC 1469 cells, GCN2iB increased NRF2, HO-1 and NQO-1 expression in a dose-dependent manner (Fig. 1G, Fig. S4). To determine whether GCN2iB affects NRF2 protein stability, we treated HepG2 cells with 50 μg/mL cycloheximide (CHX) to inhibit protein synthesis. CHX treatment decreased NRF2 expression in a time-dependent manner, but this decrease in NRF2 expression was significantly attenuated by GCN2iB (Fig. 1H).

In the livers of C57BL/6 mice, HF treatment (3 mg/kg, 3 days) decreased the protein expression of NRF2, HO-1 and NQO-1 (Fig. 1I). Compared to mice fed regular chow (nutritionally complete amino acids, Leu(+)), the hepatic protein expression of NRF2, HO-1 and NQO-1 was decreased in mice fed a leucine-deficient (Leu(−)) diet for 7 days, but the decreases in hepatic NRF2, HO-1 and NQO-1 expression caused by the Leu (−) diet were diminished in *Gcn2*$^{-/-}$ mice (Fig. 1J).

GCN2 overexpression decreases NRF2 expression in a protein-protein interaction- and KEAP1-dependent manner. Analysis with the STRING online database suggested a strong functional association between GCN2 (EIF2AK4) and NRF2 (NFE2L2) (Fig. S5). There are five conserved folded domains in the protein structure of GCN2, including an N-terminal RWD domain, a pseudokinase domain, a catalytically active kinase domain, a 'HisRS-like' domain and a C-terminal domain (CTD) [24]. To investigate the interaction between GCN2 and NRF2, the following four truncated GCN2 constructs were generated: N-terminal truncation (GCN2-N) construct, encoding AA 1–500 of GCN2; middle truncation (GCN2-M) construct, encoding AA 500–1100 of GCN2; C-terminal truncation (GCN2-C) construct, encoding AA 1010–1649 of GCN2; and GCN2-1100aa truncation (GCN2-1100aa), containing the regions of GCN2-N and GCN2-M truncations (Fig. 2A). We then transfected 293T cells with the NRF2-GFP and GCN2-Myc constructs or GCN2 truncations and performed coimmunoprecipitation (co-IP) analysis with *anti*-Myc magnetic beads. Western blot analysis showed that NRF2-GFP was only detected in the GCN2-Myc or GCN2-C-myc immunoprecipitates (Fig. 2B). In HepG2 cells expressing GCN2-C-Myc constructs, endogenous NRF2 could also be immunoprecipitated by *anti*-Myc magnetic beads (Fig. S6a). The interaction between NRF2 and the GCN2-C truncation construct was further confirmed by reciprocal immunoprecipitation assay in 293T cells expressing NRF2-Myc and GCN2-C-GFP constructs (Fig. S6b). Moreover, forced expression of GCN2-C-Myc caused an approximately decrease in the abundance of NRF2-GFP, whereas forced GCN2-N-Myc expression had no obvious effect (Fig. 2C). Although forced GCN2-*M*-Myc expression also reduced NRF2 expression, the lowering effect was weaker than that of the GCN2-C-Myc construct (Fig. 2C). Confocal microscopy images showed that when 293T cells were cotransfected with GCN2 or GCN2-C vectors, the NRF2-GFP fluorescence intensity was dramatically reduced and the remaining NRF2 was mainly located in the nucleus (Fig. 2D).

NRF2 is a short half-life protein, and its stability is mainly regulated by KEAP1, which interacts with the Neh2 domain of NRF2 by binding to ETGE and DLG motifs [10]. To determine the GCN2-binding region in NRF2, the following four NRF2 truncation constructs were generated: NRF2-Δ33aa construct, in which the KEAP1-binding motif DLG was deleted; NRF2-Δ100aa construct, in which the total Neh2 domain was deleted; N-terminal truncation (NRF2-N) construct, encoding AA 1–350 of NRF2; and C-terminal truncation (NRF2-C) construct, encoding AA 300–605 of NRF2 (Fig. 2E). Co-IP analysis revealed that GCN2-GFP was only detected in the immunoprecipitates of NRF2-Myc and NRF2-N-Myc (Fig. 2F), indicating that the DLG motif in the Neh2 domain of NRF2 is required for the interaction between GCN2 and NRF2. The interaction between GCN2 and NRF2-N truncation was further confirmed by reciprocal immunoprecipitation assay in 293T cells expressing GCN2-Myc and NRF2-N-GFP constructs (Fig. S6c). Moreover, overexpression of GCN2 significantly decreased NRF2-N-Myc expression but had no obvious effect on the expression of other truncations (Fig. 2G). Confocal microscopy images showed that NRF2-N was mainly located in the cytoplasm and NRF-C-GFP was in the nucleus. The fluorescence intensity of NRF2-N-GFP was reduced, whereas the fluorescence intensity of NRF2-C-GFP was unaffected by cotransfection with the GCN2-mCherry vector (Fig. S7).

To determine whether KEAP1 is involved in GCN2-mediated NRF2 downregulation, 293T cells were transfected with a KEAP1-specific single-guide RNA (sgRNA) expression construct plus SpCas9 expression vector (Lenti-U6-sp-KEAP1-gRNA-EFFS-spCas9-P2A-Puro), which decreased KEAP1 expression by approximately 90%. Depletion of KEAP1 significantly attenuated the GCN2-induced reduction in NRF2 expression (Fig. 2H). We next generated *KEAP1*$^{-/-}$ HepG2 cells via stable transfection with the Lent-U6-sp-KEAP1-gRNA-EFFS-spCas9-P2A-Puro lentiviral vector. Similarly, the effect of GCN2 overexpression on NRF2 reduction was almost diminished in *KEAP1*$^{-/-}$ HepG2 cells (Fig. 2I). Interestingly, co-IP analysis with *anti*-Myc magnetic beads indicated that KEAP1-GFP was detected in the GCN2-Myc immunoprecipitates, indicating that GCN2 also interacts with KEAP1 (Fig. 2J). However, co-IP analysis with *anti*-NRF2 or IgG showed that endogenous NRF2 interacted with GCN2 in both wild-type (WT) and *KEAP1*$^{-/-}$ HepG2 cells (Fig. 2K), suggesting that the interaction between NRF2 and GCN2 is independent of KEAP1.

GCN2 activation decreases NRF2 expression via a GSK-3β-dependent pathway. To determine whether protein interaction is required for GCN2 activation-mediated NRF2 reduction, 293T cells were transfected with different NRF2 truncations and then treated with 50 nM HF for 24 h. HF treatment resulted in significant decreases in the expression of NRF2-Δ100aa and NRF2-C but had no obvious effect on NRF2-N expression (Fig. 3A). To determine whether KEAP1 is involved in HF-induced downregulation of NRF2, WT and *KEAP1*$^{-/-}$ HepG2 cells were treated with 100 nM HF for 24 h. After treatment, there were similar decreases in NRF2 expression in WT and *KEAP1*$^{-/-}$ cells (Fig. 3B). These results suggested that neither the interaction between GCN2 and NRF2 nor KEAP1 is required for HF-induced NRF2 reduction.

In addition to KEAP1, dimeric β-transducin repeat-containing protein (β-TrCP) also controls NRF2 stability by binding to the Neh6 domain of NRF2, and the binding of β-TrCP to NRF2 is controlled by GSK-3β [25–27]. Therefore, we examined the effect of HF treatment on GSK-3β phosphorylation. In HepG2 and NCTC 1469 cells, HF treatment decreased the phosphorylation of GSK-3β at serine 9 in a dose-dependent

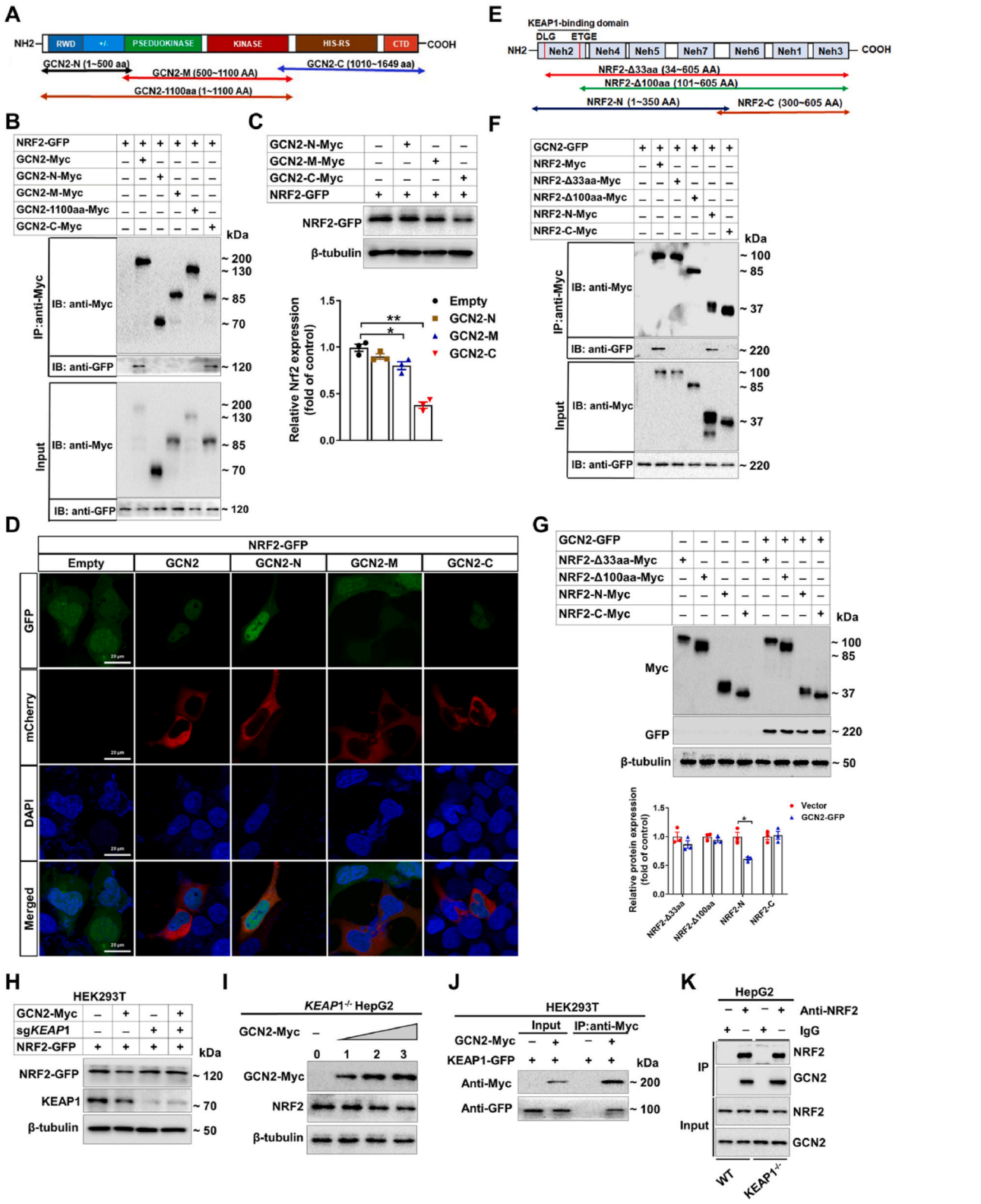

(caption on next page)

Fig. 2. GCN2 interacts with NRF2 and decreases its expression via protein-protein interactions. (A) Protein domain diagrams of GCN2 and its truncation constructs. (B) Lysates of 293T cells transfected with NRF2-GFP plus different GCN2 truncation constructs were subjected to immunoprecipitation (IP) with *anti*-Myc magnetic beads, and the resulting immunoprecipitates (IPs) as well as cell lysates used for IP (Input) were subjected to Western blot analysis with antibodies against the indicated tags. (C) Lysates of 293T cells transfected with NRF2-GFP plus different GCN2 truncation constructs were subjected to Western blot analysis. (D) 293T cells were cotransfected with NRF2-GFP and an empty vector, mCherry-tagged GCN2 or GCN2 truncation constructs, and cells were then examined by confocal microscopy. Scale bar=20 μm. (E) Protein domain diagrams of NRF2 and its truncation constructs. (F) Lysates of 293T cells transfected with GCN2-GFP plus different NRF2 truncations were subjected to IP analysis as in (B). (G) Lysates of 293T cells transfected with GCN2-GFP plus different NRF2 truncation constructs were subjected to Western blot analysis. (H) 293T cells expressing NRF2-GFP were cotransfected with GCN2-Myc and/or single guide RNA (sgRNA) targeting the KEAP1 expression construct plus the SpCas9 expression vector for 24 h. Cells were then lysed and subjected to Western blot analysis. (I) *KEAP1*$^{-/-}$ HepG2 cells were transfected with various amounts (1 × , 2 × and 3 ×) of GCN2-Myc vector for 24 h. Cells were then lysed and subjected to Western blot analysis. (J) Lysates of 293T cells cotransfected with KEAP1-GFP plus GCN2-Myc were subjected to IP analysis. (K) Lysates from WT and *KEAP1*$^{-/-}$ HepG2 cells were subjected to IP analysis with *anti*-NRF2 antibody or IgG. Independent experiments were performed at least 3 times. In Figure C and G, N=3. Values represent the mean ± SEM; * indicates $p<0.05$; ** indicates $p<0.01$.

manner (Fig. 3C, Fig. S8). On the other hand, GCN2iB increased *p*-GSK-3β^{ser9} levels in HepG2 cells in a dose-dependent manner (Fig. 3D). As a serine/threonine kinase, it is unlikely that GCN2 directly induces dephosphorylation of GSK-3β. Therefore, we investigated whether GCN2-inactivated kinases regulate GSK-3β phosphorylation. It has been reported that GCN2 sustains mammalian target of rapamycin (mTOR)/70-kDa ribosomal S6 kinase 1 (p70S6K1) suppression upon amino acid deprivation [28] and that p70S6K1 inhibits GSK-3β activity via phosphorylation at serine 9 [29]. Thus, we examined the phosphorylation of p70S6K1 at threonine 389 in HepG2 cells. As expected, HF treatment decreased the p-p70S6K1^{T389} levels in HepG2 cells, but GCN2iB increased the p-p70S6K1^{T389} levels in HepG2 cells (Fig. 3C and D). In HepG2 cells, the HF-induced decreases in NRF2 expression and the phosphorylation of GSK-3β were attenuated by GCN2iB or the CHIR-99021 (CHIR) GSK-3β-specific inhibitor (Fig. 3E).

GSK-3β has been reported to decrease NRF2 expression by phosphorylating groups of serine residues in the Neh6 region of NRF2, including S347, S356, S361 and S383 [25–27]. To determine whether these serine residues are required for HF-induced NRF2 reduction, several of the serine residues were mutated as alanine residues, including S347A, S347A/S356A, S347A/S356A/S361A, S347A/S356A/S383A and S347A/S356A/S361A/S383A. Western blot analysis showed that HF treatment resulted in a similar degree of reduction in WT-NRF2 and S347A expression but caused less reduction in the expression of other mutations (Fig. 3F), indicating that mutation in these serine residues decreased the sensitivity of NRF2 to HF treatment.

Interestingly, mutation of serine residues did not affect the GCN2 overexpression-induced decrease in NRF2 expression (Fig. S9). However, overexpression of the GCN2-M truncation did not decrease the expression of the S347A/S356A/S361A/S383A mutation (NRF2-4S/4A) in 293T cells. Moreover, the reduction in NRF2 expression caused by overexpression of GCN2-M truncation was blocked by GCN2iB and CHIR (Fig. S10).

The Leu (−) diet decreased the phosphorylation of GSK-3β and p70S6K1 in the livers of WT mice but significantly increased the *p*-GSK-3β and p-p70S6K1 levels in the livers of *Gcn2*$^{-/-}$ mice (Fig. 3G). Inhibition of GSK-3β by CHIR increased NRF2 expression and GSK-3β phosphorylation in the livers of mice fed a Leu (−) diet (Fig. 3H), indicating that Leu (−) diet-induced activation of hepatic GSK-3β decreases NRF2 expression.

GCN2 repressed NRF2 transcriptional activity under stress conditions. To investigate the effect of GCN2 on NRF2 transcriptional activity, sh*GCN*2 or shRNA lentiviral vector targeting a scrambled sequence (shScr) stably transfected HepG2 cells were treated with 100 μM H_2O_2 for 24 h. Knockdown of GCN2 attenuated the phosphorylation of eIF2α in H_2O_2-treated cells (Fig. S11). After H_2O_2 treatment, NRF2 was translocated from the cytoplasm to the nucleus, and the mRNA levels of NRF2 downstream target genes (*GCLM*, *GSTM*1, *GSTA*1 and *GPX*1) were significantly increased. H_2O_2-induced NRF2 nuclear translocation and the upregulation of NRF2 downstream target genes were further promoted by GCN2 knockdown (Fig. 4A and B). Knockdown of GCN2 increased the viability of H_2O_2-treated cells (Fig. 4C). When NRF2 was depleted by an NRF2-specific shRNA lentiviral vector (sh*NRF*2), the protective effect of GCN2 knockdown on cell viability loss was diminished (Fig. 4D). In control HepG2 cells, GCN2 knockdown did not affect intracellular ROS levels. When cells were treated with 200 μM H_2O_2, the increase in intracellular ROS levels was significantly attenuated by GCN2 knockdown (Fig. 4E). When NRF2 was depleted, GCN2 knockdown still decreased intracellular ROS levels in H_2O_2-treated cells (Fig. 4F). We also found that GCN2iB increased, whereas HF decreased, HO-1 and NQO-1 expression in H_2O_2-treated cells, (Fig. 4G). Moreover, GCN2iB attenuated, while HF exacerbated, the H_2O_2-induced loss of cell viability (Fig. 4H). Together, these data suggested that GCN2 negatively regulated NRF2 transcriptional activity under oxidative stress conditions, thereby rendered cells more vulnerable to H_2O_2-induced cell death.

Knockdown of *Gcn*2 alleviates insulin resistance, hepatic steatosis and oxidative stress in ob/ob mice. To investigate whether depletion of *Gcn*2 alleviates NAFLD in an NRF2-dependent manner, we depleted *Gcn*2 and/or *Nrf2* from the livers of ob/ob mice via tail vein injection of the adeno-associated virus serotype 8 (AAV8)-sh*Gcn*2 and/or AAV8-shNrf2 vectors. Mice that received AAV8-GFP injection were used as controls. Knockdown of *Gcn2* decreased serum aspartate aminotransferase (AST), aminotransferase (ALT), nonesterified fatty acid (NEFA) and insulin levels but increased serum high-density lipoprotein cholesterol (HDL-C) levels. *Nrf2* knockdown increased serum AST, ALT, NEFA and insulin levels but decreased serum HDL-C levels. Moreover, the effect of *Gcn2* knockdown on these serum biochemical indexes was diminished when *Nrf2* was depleted (Fig. 5A–E). The results of the oral glucose tolerance test (OGTT) and insulin tolerance test (ITT) revealed that GCN2 knockdown increased glucose excretion and insulin sensitivity as indicated by the decreased area under the curve (AUC) values (Fig. 5F–G). However, the GCN2 knockdown-induced improvements in glucose tolerance and insulin sensitivity were abolished by NRF2 knockdown. Hematoxylin and eosin (H&E), oil red O and DHE staining showed that *Gcn2* knockdown ameliorated liver injury, steatosis and superoxide production in ob/ob mice (Fig. 5H). *Gcn2* knockdown decreased triglyceride (TG), total cholesterol (TC), NEFA, 3′-nitrotyrosine (3′-NT) and 4-hydroxynonenal (4-HNE) levels but increased the ratio of reduced glutathione (GSH)-to-oxidized glutathione (GSSG) in the livers of ob/ob mice (Fig. 5I-N). Knockdown of *Nrf2* not only caused more liver injury, steatosis and oxidative stress in the livers of ob/ob mice, but also abolished the *Gcn2* knockdown-mediated decreases in liver TG, TC, NEFA, 3′-NT and 4-HNE levels as well as increase in GSH/GSSG ratio (Fig. 5H-N). Western blot analysis demonstrated that AAV8-sh*Gcn*2 decreased hepatic GCN2 expression by approximately 60%. Furthermore, *Gcn2* knockdown increased the protein expression of NRF2, HO-1, NQO-1, KEAP1 and *p*-GSK-3β. In contrast, *Nrf2* knockdown resulted in significant decreases in the protein expression of NRF2, HO-1, NQO-1 and *p*-GSK-3β (Fig. 5O). Knockdown of *Nrf2* did not affect the *Gcn2* knockdown-induced increases in the protein expression of NRF2, HO-1 and *p*-GSK-3β, but it abolished the changes in the protein expression of KEAP1 and NQO-1 (Fig. 5O).

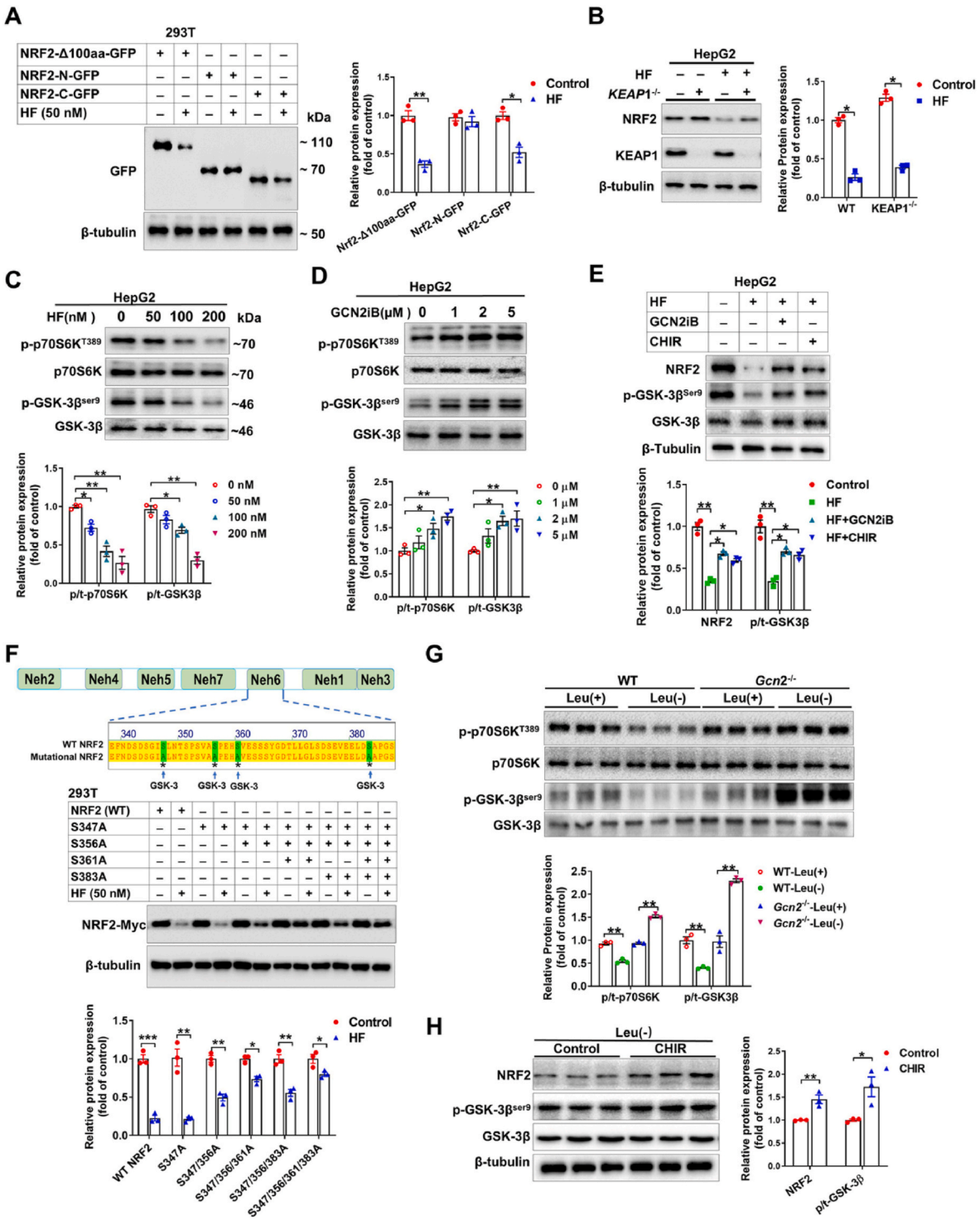

Fig. 3. GCN2 activity affects NRF2 expression by regulating the phosphorylation of GSK-3β. (A) 293T cells transfected with different NRF2 truncation constructs were treated with 50 nM HF for 24 h, and cell lysates were then examined by Western blot analysis. (B) WT and *KEAP1*$^{-/-}$ HepG2 cells were treated with 100 nM HF for 24 h, and cell lysates were then subjected to Western blot analysis. (C) HepG2 cells were treated with 0–200 nM HF for 24 h. Cell lysates were then subjected to Western blot analysis. (D) HepG2 cells treated with 0–5 μM GCN2iB were lysed and subjected to Western blot analysis. (E) HepG2 cells were cotreated with 100 nM HF and 2 μM GCN2iB or CHIR for 24 h, and the cell lysates were then examined by Western blot analysis. (F) Diagram shows the serine residues in the Neh6 domain of human NRF2 that are predicted to be phosphorylated by GSK-3β. 293T cells transfected with WT or mutated NRF2 constructs were treated with 50 nM HF for 24 h, and the cell lysates were then examined by Western blot analysis. (G) Mice were fed a Leu (+) or Leu (−) diet for 7 days, and liver lysates were then examined by Western blot analysis. (H) WT mice fed a Leu (−) diet were administered CHIR (5 mg/kg). Liver lysates were examined by Western blot analysis. N=3, values represent the mean ± SEM; * indicates $p<0.05$; ** indicates $p<0.01$; *** indicates $p<0.001$.

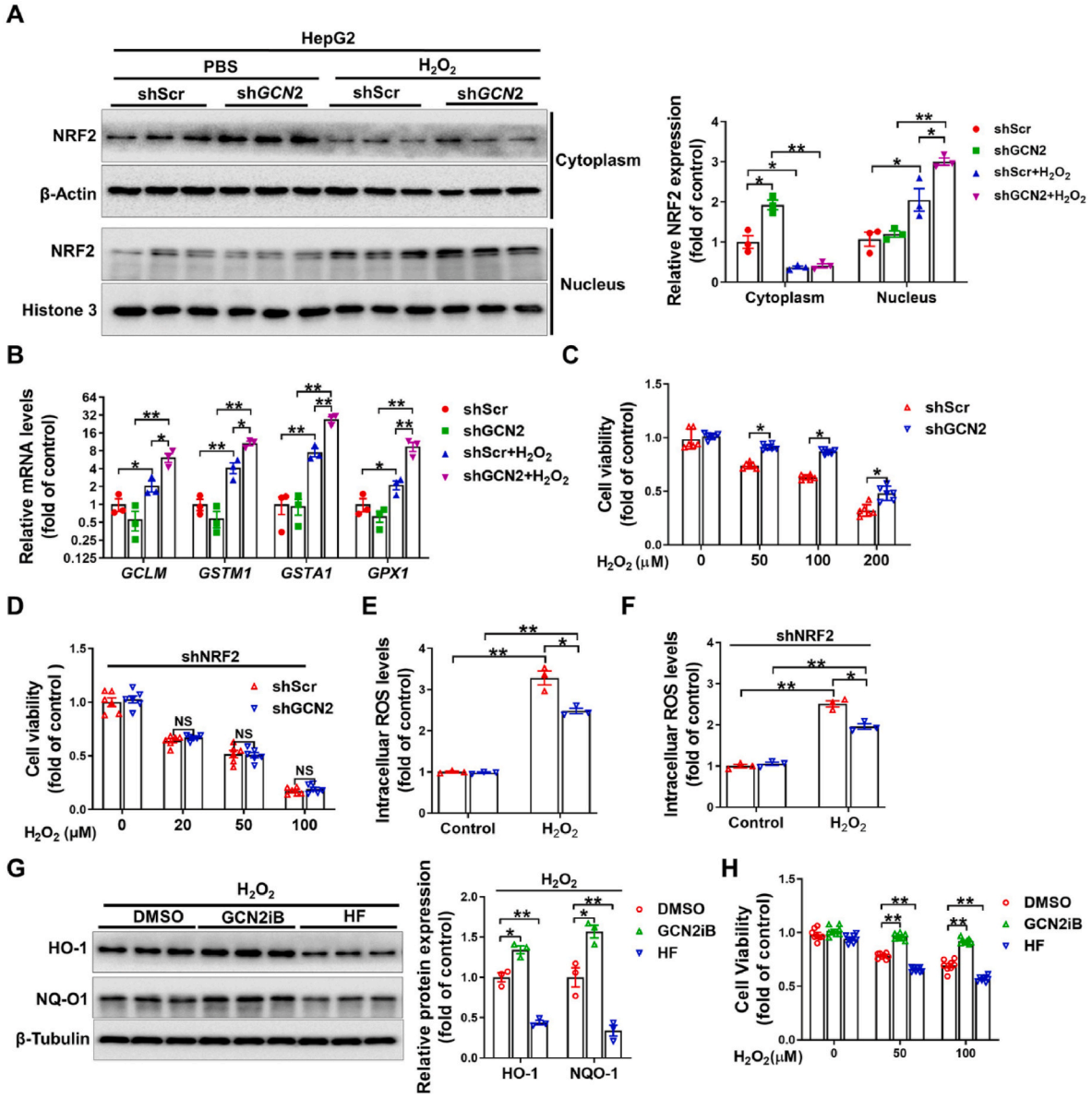

Fig. 4. Gcn2 inhibits NRF2 transcriptional activity under stress conditions. (A, B) HepG2 cells were stably transfected with shScr or shGCN2. After incubation with 100 μM H_2O_2 for 24 h, NRF2 in the cytoplasm and nucleus was examined by Western blot analysis (A), and the mRNA levels of NRF2 downstream target genes were measured by quantitative real-time PCR (B). (C) HepG2 cells were treated with 0–200 μM H_2O_2 for 24 h, and cell viability was measured by MTT assay. (D) HepG2 cells were transfected with shRNA lentiviral vector targeting NRF2 (sh*NRF2*). After incubation with 0–100 μM H_2O_2 for 24 h, cell viability was measured. (E) The intracellular levels of reactive oxygen species (ROS) in control or 200 μM H_2O_2-treated cells were measured. (F) HepG2 cells transfected with sh*NRF2* were treated with 50 μM H_2O_2 for 24 h, and the intracellular ROS levels were measured. (G) Lysates of HepG2 cells treated with 50 μM H_2O_2 plus GCN2iB (2 μM) or HF (50 nM) were examined by Western blot analysis. (H) After treatment with H_2O_2 and GCN2iB (2 μM) or HF (50 nM) for 24 h, cell viability was measured. In Figure A, B, E-G, N=3; in Figure C, D and H, N=8. Values are the mean ± SEM; * indicates $p<0.05$; ** indicates $p<0.01$.

Gcn2 knockdown significantly decreased the mRNA levels of stearoyl-CoA desaturase-1(*Scd1*), sterol regulatory element binding transcription factor 1 (*Srebp1c*), fatty acid synthase (*Fasn*) and peroxisome proliferator activated receptor gamma (*Pparg)* but increased the mRNA levels of *Ppara* and acyl-CoA oxidase 1 (*Acox1*). However, these changes were abolished by *Nrf2* knockdown (Fig. S12).

Inhibition of NRF2 diminishes the effect of GCN2 knockdown on palmitic acid-induced lipid accumulation in HepG2 cells. In palmitic acid (PA)-treated (0.25 mM, 24 h) HepG2 cells, GCN2 knockdown significantly attenuated lipid accumulation (as monitored by Nile red staining). ML385 is an inhibitor of NRF2 that binds the Neh1 domain of NRF2 and inhibits its downstream target gene expression [30]. When PA-treated cells were coincubated with 2 μM ML385, there was no significant difference in the Nile red fluorescence intensity between GCN2-depleted and control cells (Fig. S13), indicating that inhibition of NRF2 blunts the protective effect of GCN2 knockdown on lipid accumulation.

Inhibition of GCN2 ameliorates insulin resistance, hepatic steatosis and oxidative stress in obese mice. To determine whether inhibition of GCN2 is a potential therapeutic approach for NAFLD, we treated ob/ob mice and HFD-fed mice with GCN2iB (3 mg/kg) every other day for 6 weeks. Oil-treated mice were used as control. At the end of the experiments, GCN2iB-treated ob/ob and HFD-fed mice exhibited significantly lower serum ALT, AST, NEFA and insulin levels but higher HDL-C levels than oil-treated mice (Fig. 6A–E). GCN2iB treatment also increased glucose tolerance and insulin sensitivity in both ob/ob and HFD-fed mice (Fig. 6F–I). As revealed by H&E, oil red O and DHE staining, liver injury, steatosis and superoxide production in both ob/ob

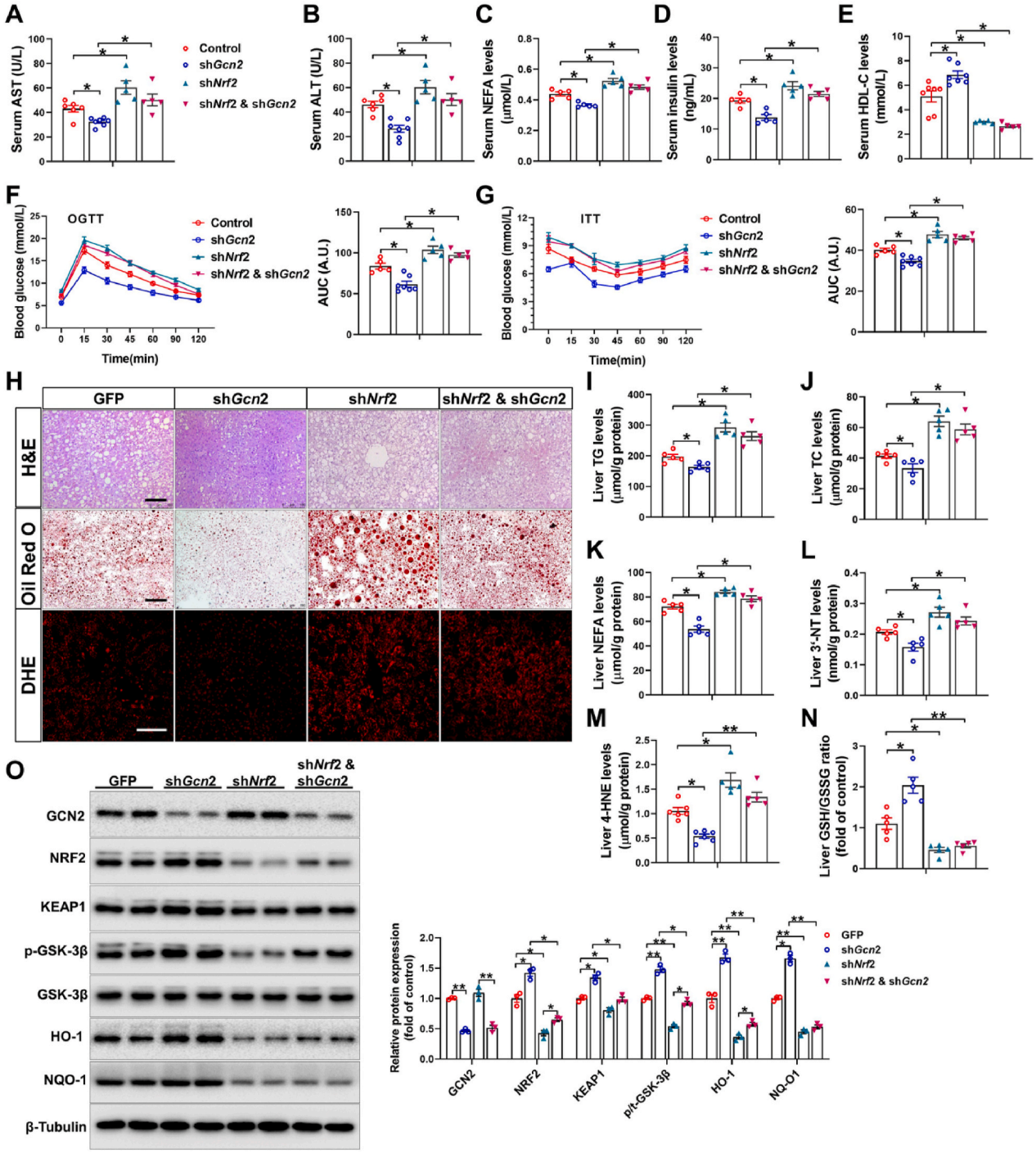

Fig. 5. GCN2 knockdown ameliorates hepatic steatosis and oxidative stress in ob/ob mice in an NRF2-dependent manner. (A–E) Ob/ob mice were treated with AAV8-GFP, AAV8-sh*Gcn2*, AAV8-sh*Nrf2* or AAV8-sh*Nrf2* & AAV8-sh*Gcn2* via tail vein injection. At 4 weeks after injection, the mice were sacrificed, and serum aspartate transaminase (AST) (A), alanine transaminase (ALT) (B), nonesterified fatty acid (NEFA) (C), insulin (D) and high-density lipoprotein cholesterol (HDL-C) (E) levels were measured. (F, G) Oral glucose tolerance tests (OGTTs) (F) and insulin tolerance tests (ITTs) (G) were performed on GFP-, sh*Gcn2* sh*Nrf2*-and sh*Nrf2* & sh*Gcn2*-treated ob/ob mice, and the corresponding area under the curve (AUC) values for blood glucose levels in each group were calculated. (H) Representative liver sections were stained with hematoxylin and eosin (H&E), oil red O and dihydroethidium (DHE). Scale bar = 100 μm. (I–N) Liver triglyceride (TG) (I), total cholesterol (TC) (J), NEFA (K), 3′-nitrotyrosine (3′-NT) (L) and 4-hydroxynonenal (4-HNE) (M) levels as well as the ratio of reduced glutathione to oxidized glutathione (GSH/GSSG) (N) were measured. (O) Liver lysates were examined by Western blot analysis. In Figure A–N, N=5. In Figure O, N=3. Values represent the mean ± SEM; * indicates $p<0.05$; ** indicates $p<0.01$. (For interpretation of the references to colour in this figure legend, the reader is referred to the Web version of this article.)

and HFD-fed mice were improved by GCN2iB treatment (Fig. 6J). Moreover, GCN2iB decreased liver TG, TC, 3′-NT, 4-HNE and GSSG levels but increased liver GSH levels and the GSH/GSSG ratio in ob/ob and HFD-fed mice (Fig. 6K-O, Fig. S14). Western blots analyses showed that the expression of NRF2 and *p*-GSK-3β expression was increased, while the expression of FAS, CD36 and CIDEA was decreased in the livers of GCN2iB-treated mice (Fig. 6P).

Inhibition of GCN2 attenuates lipid accumulation in PA- and oleic acid-treated cells. To further confirm that GCN2iB affects lipid accumulation in hepatocytes, we used PA- or oleic acid (OA)-treated

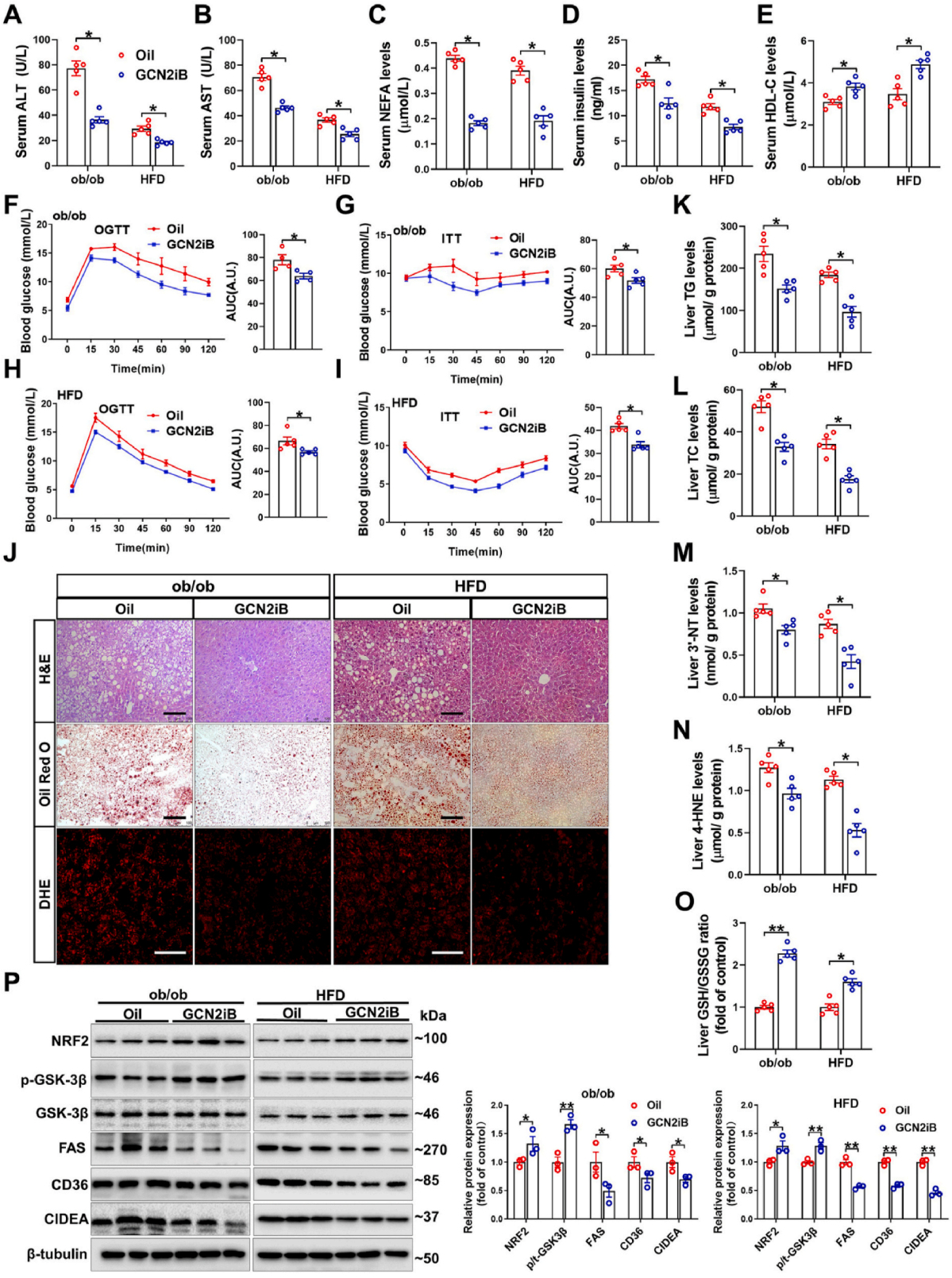

Fig. 6. GCN2iB ameliorates insulin resistance, hepatic steatosis and oxidative stress in obese mice. (A–E) Ob/ob mice and C57BL/6 mice fed a high-fat diet (HFD) for 16 weeks were treated with oil or GCN2iB (3 mg/kg) every other day for 6 weeks. After the mice were sacrificed, serum ALT (A), AST (B), NEFA (C), insulin (D) and HDL-C (E) levels were measured. (F–I) OGTT and ITT were performed on oil- and GCN2iB-treated ob/ob mice (F, G) as well as HFD-fed mice (H, I), and the corresponding AUC values for blood glucose levels in each group were calculated. (J) Representative liver sections from oil- and GCN2iB-treated obese mice were stained with H&E, oil red O and DHE. Scale bar = 100 μm. (K–O) Liver TG (K), TC (L), 3′-NT(M) and 4-HNE (N) levels as well as the GSH/GSSG ratio (O) were measured. (P) Liver lysates from oil- and GCN2iB-treated obese mice were examined by Western blot analysis. In Figure A–N, N=5. In Figure P, N=3. Values represent the mean ± SEM; * indicates $p<0.05$; ** indicates $p<0.01$. (For interpretation of the references to colour in this figure legend, the reader is referred to the Web version of this article.)

L02 cells as *in vitro* NAFLD models. Nile red staining demonstrated that GCN2iB significantly attenuated lipid accumulation in PA- or OA-treated L02 cells (Fig. S15a). GCN2iB also decreased FAS and CIDEA expression in PA- and OA-treated L02 cells (Fig. S15b).

GCN2iB affects hepatic metabolites in HFD-fed mice. To investigate the effect of GCN2iB on hepatic metabolism, nontargeted metabolomics approaches were performed to measure the metabolites in the liver of HFD-fed mice. As revealed by the principal component analysis (PCA) and the supervised orthogonal projections to latent structures-discriminant analysis (OPLS-DA) score plots, the primary metabolic components were different between the oil- and GCN2iB-treated groups (Fig. 7A). With the selection criterion of variable importance in the projection (VIP) > 1.0 and Student's t-test p value < 0.05, 926 differential metabolites (531 increased and 395 decreased) were identified, and the fold changes of these metabolites were visualized in volcano plots (Fig. 7B). The differential metabolites were divided

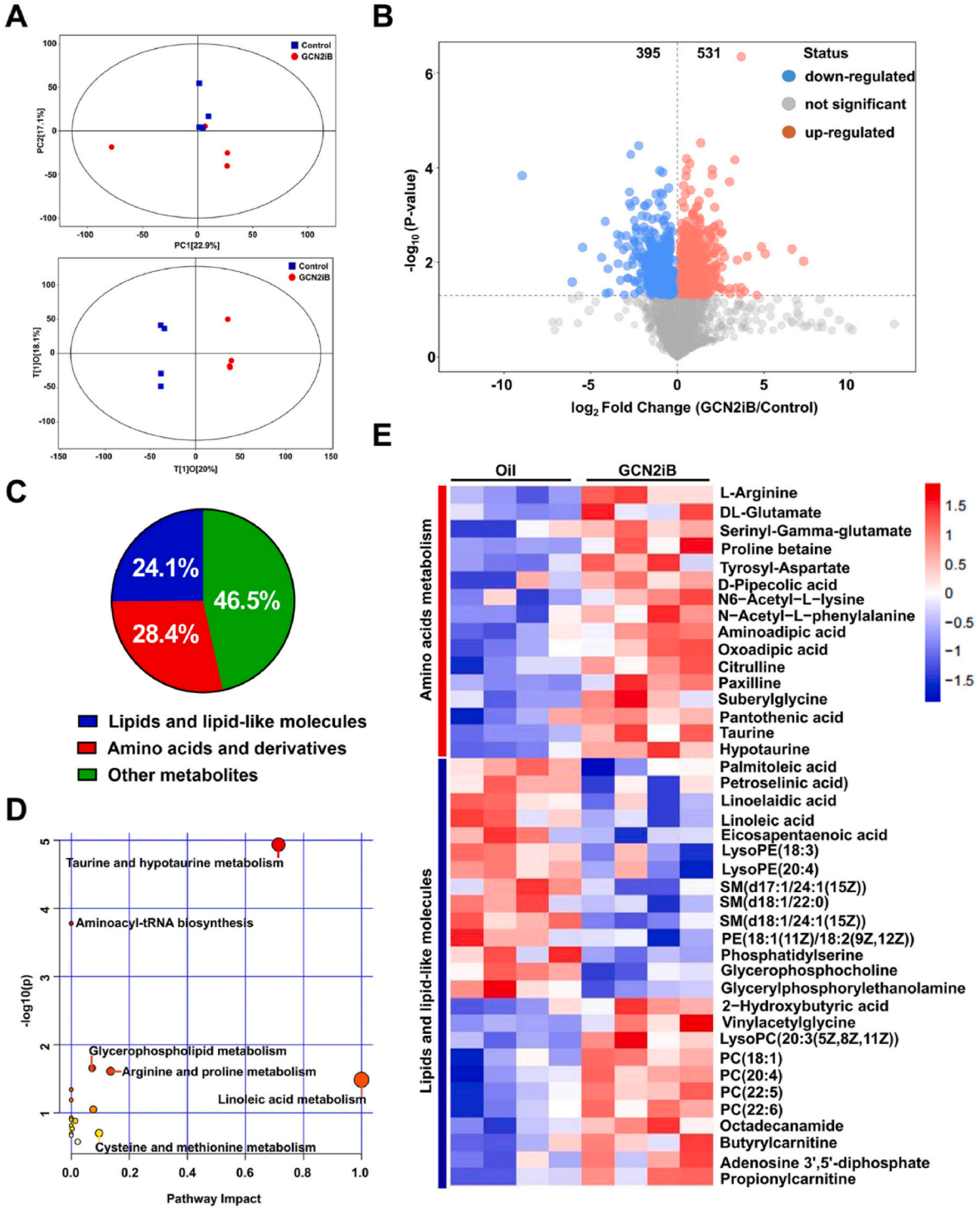

Fig. 7. GCN2iB affects liver metabolomic profiles in HFD-fed mice. (A) The principal component analysis (PCA) model (upper panel) and the orthogonal projections to latent structures-discriminant analysis (OPLS-DA) (lower panel) model for the oil- and GCN2iB-treated groups are presented as score scatter plots. (B) The changes in hepatic metabolites in HFD-fed mice are presented in a volcano plot. (C) The percentages of major metabolites are illustrated in a pie chart. (D) KEGG pathway analysis of the significantly different metabolites. (E) The significantly changed amino acid- and lipid-related metabolites are presented as a heatmap.

into the following three categories: lipids and lipid-like molecules (24.1%); amino acids and derivatives (28.4%); and others (46.5%) (Fig. 7C). With the selection criterion of VIP >1.0 and false discovery ratio (FDR)-adjusted p value < 0.05, 97 differential metabolic signatures were screened. We then used MetaboAnalyst software (version 5.0, http://www.metaboanalyst.ca/) to map the identified metabolites to their corresponding physiologic pathways. KEGG pathway enrichment analysis showed that the perturbed metabolic pathways in the GCN2iB group mainly were related to the following functions: taurine and hypotaurine metabolism; glycerophospholipid metabolism; linolenic acid metabolism; aminoacyl-tRNA biosynthesis; cysteine and methionine metabolism; and arginine and proline metabolism (Fig. 7D). The relative levels of metabolites involved in amino acid metabolism as well as lipids and lipid-like metabolism between the oil- and GCN2iB-treated groups were visualized in a heatmap (Fig. 7E). GCN2iB treatment significantly increased the levels of amino acid-related metabolites (e.g., L-arginine, DL-glutamate, citrulline, taurine and hypotaurine), phosphatidylcholine (e.g., lysoPC (20:3), PC (18:1), PC (20:4), PC (22:5) and PC

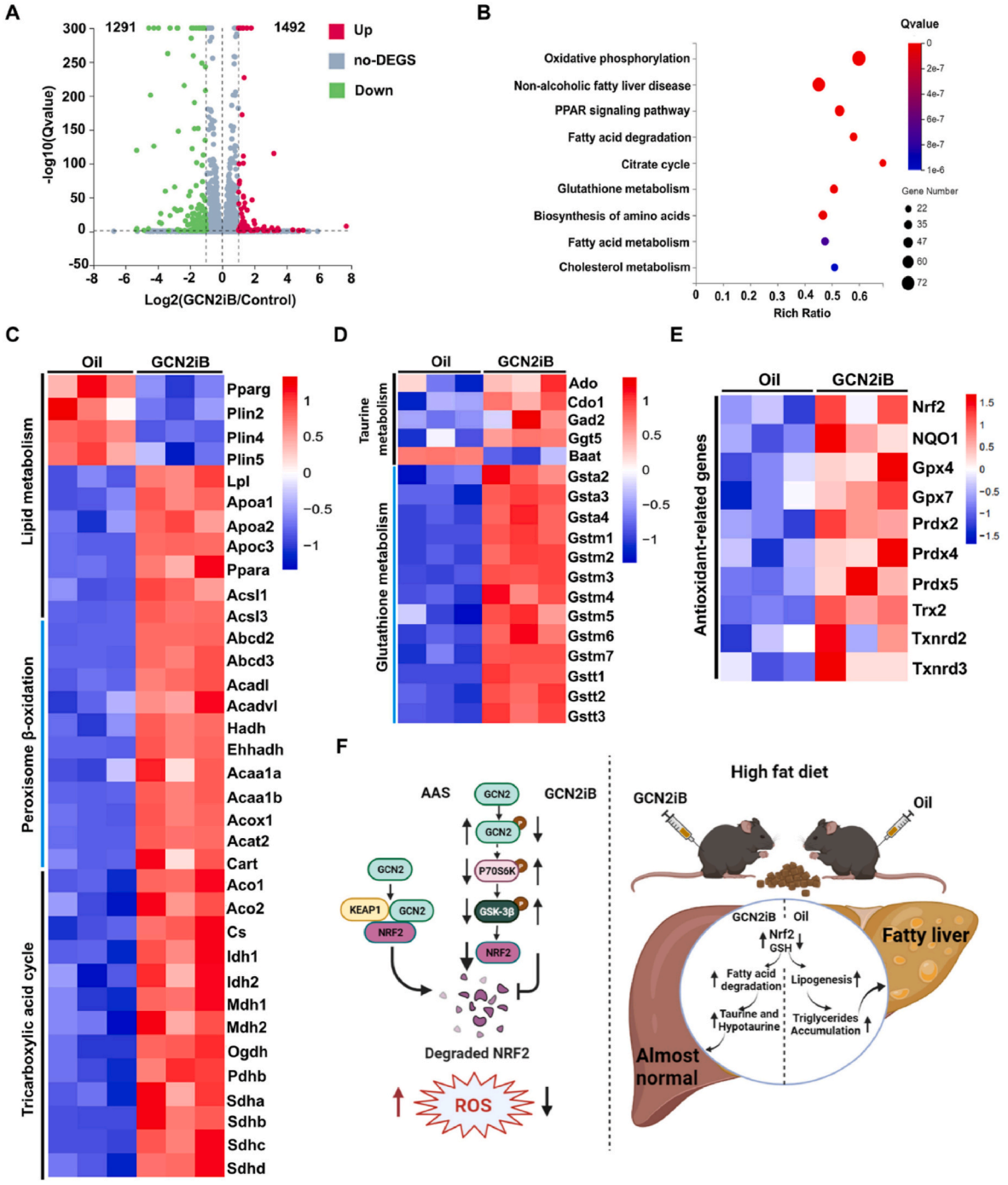

Fig. 8. GCN2iB affects gene expression profiles in HFD-fed mice. (A) The fold changes in the expression of differentially expressed genes (DEGs) in the control group vs. GCN2iB group are presented in a volcano plot. (B) The advanced bubble chart shows the top 9 significantly enriched KEGG pathways of the DEGs in the control group vs. GCN2iB group. (C) The gene expression profiles of the DEGs that were involved in lipid metabolism, peroxisome β-oxidation and tricarboxylic acid cycle pathways are shown in the heatmap. (D, E) The gene expression profiles of the DEGs that were involved in glutathione metabolism and the NRF2 pathway are shown in the heatmap. (F) Schematic diagram showing the main findings of this manuscript.

(22:6)) levels but decreased fatty acid (e.g., palmitoleic acid, petroselinic acid, linelaidic acid and linoleic acid), lysophospholipid (lysoPE (18:3) and lysoPE (20:4)) and sphingomyelin (SM(d17:1/24:1(15z)), SM (d18:1/20:0) and SM(d18:1/24:1(15z))) levels in the fatty livers.

GCN2iB affects the gene expression profile in the livers of HFD-fed mice. To further investigate the protective mechanism of GCN2iB, RNA sequencing was performed to analyze the global gene expression profiling changes. We identified 2783 differentially expressed genes (DEGs) (1492 upregulated and 1291 downregulated) in the control group vs. GCN2iB group, and the fold changes of these DEGs were visualized in a volcano plot (Fig. 8A). Moreover, Kyoto Encyclopedia of Genes and Genomes (KEGG) enrichment analysis showed that these DEGs were mainly enriched in lipid- and amino acid metabolism-related pathways, including oxidative phosphorylation, nonalcoholic fatty liver disease, PPAR signaling pathway, fatty acid degradation, citrate cycle, biosynthesis of amino acids and glutathione metabolism pathway (Fig. 8B). In fatty acid-metabolism related DEGs, the expression of *Pparg* and perilipin 2/4/5 was reduced, while the expression of lipoprotein lipase (*Lpl*), apolipoprotein A1/A2 (*Apoa1/2*), *Ppara* and acyl-CoA synthetase long chain family member 1/3 (*Acsl*1/3) was increased in GCN2iB group (Fig. 8C). GCN2iB treatment also increased the expression of a series of genes involved in peroxisome β-oxidation (e.g., *Abcd2/3*, *Acadl*, *Acadvl* and *Hadh*), citric acid cycle (e.g., *Aco1/2*, *Cs* and *Idh1/2*), taurine (*Ado*, *Cdo1*, *Gad2*, *Ggt5* and *Batt*) and glutathione (*Gsta2/3/4*, *Gstm1-7* and *Gstt1/2/3*) metabolism (Fig. 8D–E). Consistently, NRF2 and its downstream targets (e.g., *Nqo-1*, *Gpx4*, *Gpx7*, *Prdx2* and *Prdx4*) were upregulated in the GCN2iB group (Fig. 8F). To validate the RNA-seq results, we measured several genes involved in lipid, glutathione and taurine metabolism. We found that GCN2iB significantly decreased the mRNA levels of *Pparg* and increased the mRNA levels of *Ppara*, *Acox1*, glutathione S-transferase alpha 1 (*Gsta1*), glutathione S-transferase Mu 1 (*Gstm1*), glutathione S-transferase Theta 1 (*Gstt1*), glutathione peroxidase 4 (*Gpx4*), 2-aminoethanethiol dioxygenase (*Ado*), cysteine dioxygenase type 1 (*Cdo1*), glutamate decarboxylase 2 (*Gad2*) and gamma-glutamyltransferase 5 (*Ggt5*) (Fig. S16).

Together, these results indicated that the protective effects of GCN2iB on hepatic steatosis and oxidative stress in fatty livers are linked to activation of the NRF2 pathway, enhanced degradation of fatty acids and synthesis of taurine and glutathione.

3. Discussion

There are two major new findings in the present study. First, we demonstrated that GCN2 negatively regulates the NRF2 pathway via protein-protein interactions or activation of GSK-3β. Second, GCN2iB effectively protects against hepatic steatosis, oxidative stress in obese mice, which is associated with activating NRF2 pathway.

Although GCN2 is known for its role in maintaining amino acid homeostasis, there is evidence that GCN2 also participates in the control of cellular redox status under different conditions [18,31,32]. However, the underlying mechanism by which GCN2 regulates oxidative stress remains elusive. It has been reported that GCN2 activation by HF suppresses NRF2 accumulation in some cancer cells [22], while GCN2 knockdown enhances NRF2 pathway activation in high glucose-treated ARPE-19 cells [21]. Here, we showed that NRF2 expression was negatively associated with GCN2 expression and/or activity in HepG2 cells. GCN2 knockdown promoted NRF2 nuclear translocation and attenuated cell death in H_2O_2-treated cells, and the protective effect of GCN2 depletion was diminished by knockdown of NRF2. In addition, GCN2 knockdown increased NRF2 expression and alleviated hepatic oxidative stress in ob/ob mice in an NRF2-dependent manner. These results suggested that the impact of GCN2 on the hepatic redox state is tightly associated with changes in the NRF2 signaling pathway.

It is well recognized that KEAP1 negatively regulates the stability of NRF2 through the formation of the ubiquitylation-competent KEAP1-NRF2 complex. Some proteins, such as p62/sequestosome-1 and $p21^{Cip1/WAF1}$, interact with KEAP1 or NRF2 and then influence the NRF2 signaling pathway by interfering with the NRF2-KEAP1 complex [33,34]. Interestingly, both GCN2 and KEAP1 bind to the Neh2 domain of NRF2, and the KEAP1-binding motif, DLG, is also required for the GCN2-NRF2 interaction. Because GCN2 also interacts with KEAP1 and GCN2-mediated NRF2 reduction is diminished by KEAP1 deletion, it is likely that GCN2 behaves as an interactive hub to reinforce KEAP1-dependent NRF2 degradation rather than disrupt the NRF2-KEAP1 complex.

The present study showed that HF decreased NRF2 expression in *KEAP1*$^{-/-}$ HepG2 cells, suggesting that GCN2 activation-mediated NRF2 reduction depends on a KEAP1-independent pathway. The β-TrCP/GSK-3β pathway is another well-characterized pathway that connects NRF2 degradation with growth factor signaling [25–27]. Here, we found that GCN2 activation by HF treatment or a Leu(−) diet decreased *p*-GSK-3β^{ser9} levels in HepG2 cells and livers, while GCN2 inhibition by GCN2iB or *Gcn2* deletion/depletion increased *p*-GSK-3β^{ser9} levels in HepG2 cells and livers. Moreover, inhibition of GSK-3β by CHIR restored NRF2 expression in GCN2-activating cells and livers. Mutation of the phosphorylation sites of GSK-3β in the Neh6 domain of NRF2 attenuated HF-induced NRF2 reduction. Unlike most kinases, the activity of GSK-3β is inhibited by phosphorylation at serine 9 by protein kinase B (PKB)/Akt [35] or p70S6K1 [29]. Because amino starvation induced-GCN2 activation repressed p70S6K1, we hypothesized that GCN2 indirectly activates GSK-3β via inhibition of p70S6K1.

The reason why GCN2 affects NRF2 expression via two different mechanisms might be due to the structural rearrangement during the activation of GCN2. In non-starved cells, multiple autoinhibitory interactions occur among the CTD, HisRS-like domains and kinase domains to maintain GCN2 in an inactive dimeric state [36]. Interestingly, the HisRS-like and CTD domains are required for the interaction between GCN2 and NRF2 and GCN2 overexpression-mediated NRF2 reduction. Upon amino acid starvation, the binding of accumulated deacylated tRNA to the HisRS-like domain causes a disruption of these multi-domain autoinhibitory contacts and facilitates the interaction between the kinase and pseudokinase domains [36,37]. Whether the conformational changes in HisRS-like and CTD domains affect the protein interaction between GCN2 and NRF2 is unclear. Since deletion of the CTD domain increases the *in vitro* kinase activity of GCN2 by ~20-fold [38], it is reasonable that GCN2-M truncation decreases NRF2 expression through increasing kinase activity.

We previously demonstrated that *Gcn2* deficiency attenuates HFD-induced liver dysfunction, hepatic steatosis, insulin resistance and the upregulation of lipogenesis genes [20]. Here, we also found that AAV8-sh*Gcn2* alleviated hepatic steatosis and insulin resistance in ob/ob mice. In addition, *Gcn2* knockdown decreased *Srebp1c*, *Pparg*, *Fasn* and *Scd1* in the livers of ob/ob mice, suggesting a potential mechanism for the GCN2-dependent regulation of lipogenesis. NRF2 not only controls the expression of antioxidant/detoxifying genes, but also regulates genes involved in lipid metabolism [39]. Here, we found that *Gcn2* knockdown increased the expression of NRF2, and *Nrf2* knockdown diminished the protective effect of *Gcn2* knockdown on hepatic steatosis and oxidative stress. Therefore, it is likely that the detrimental role of GCN2 in fatty livers is due, in part, to repressing the NRF2 signaling pathway.

The present study also showed that GCN2iB increased NRF2 protein expression and/or stability in HepG2 cells, suggesting that GCN2iB might be a potential NRF2 activator in hepatocytes. Several NRF2 activators, including curcumin [40], quercetin [41] and TBE-31 [42], have been found to ameliorate hepatic steatosis and oxidative stress in NAFLD animal models. Here, we also found that GCN2iB alleviated NAFLD-like phenotypes in both ob/ob and HFD-fed mice, which was associated with the upregulation of NRF2 and its downstream targets. In fatty livers, GCN2iB treatment resulted in decreases in the abundance of fatty acids, lysophospholipids and sphingomyelin and increases in the abundance of phosphatidylcholine. The regulation of lipid metabolites by GCN2iB was

associated with inhibition of lipogenesis pathways and acceleration of fatty acid degradation pathways. GCN2iB may also protect against hepatic steatosis and oxidative stress by modulating the abundance of amino acid-related metabolites and upregulating antioxidant enzymes. As the most potent intrinsic antioxidant, GSH not only directly scavenges oxygen free radicals but also acts as a substrate for antioxidant enzymes. Oral administration of GSH leads to an attenuation of NAFLD in patients [43]. Here, we showed that GCN2iB increased the GSH/GSSG ratio and total glutathione levels in the livers of HFD-fed mice, which was associated with the upregulation of glutathione metabolic genes. GCN2iB also increased the abundance of citrulline and taurine, which exert beneficial effects in NAFLD animal models [44,45].

As summarized in Fig. 8F, our study demonstrated that GCN2 negatively regulates NRF2 via two different mechanisms and that inhibiting GCN2 in hepatocytes attenuates hepatic steatosis and oxidative stress in an NRF2-dependent pathway. Our results also suggested that the specific GCN2 inhibitors may be potential drug candidates for NAFLD therapy.

4. Materials and methods

Detailed materials and methods are available in the online-only data Supplement.

4.1. Animals and experimental design

Gcn2$^{-/-}$ mice [46] were obtained from The Jackson Laboratory (stock No: 008240, Bar Harbor, ME, USA). C57BL/6 and ob/ob mice were purchased from Vital River Laboratories (Beijing, China) and HFK Bioscience Co. (Beijing, China), respectively. All animals were housed in the individually ventilated cage systems at 22 °C with a 12 h light/dark cycle, and they had free access to rodent chow and tap water. Animal studies were performed in accordance with the Guide for the care and use of laboratory animals (Eighth edition, 2011) and the approval of the University of Chinese Academy of Sciences Animal Care and Use Committee.

For HF treatment, 8-week-old male C57BL/6 mice were intraperitoneally injected with 3 mg/kg HF, and mice were then sacrificed after 3 days. For leucine deprivation experiments, 8-week-old male *Gcn2*$^{-/-}$ mice and WT littermates were provided with either control (nutritionally complete amino acids, Leu(+)) or leucine-deficient (Leu(−)) diets for 7 days. Male ob/ob mice aged 8–10 weeks were used for other experiments. Hepatic *Gcn2* and *Nrf2* knockdown in ob/ob mice was accomplished by tail vein injection of AAV8-sh*Gcn2* and AAV8-sh*Nrf2* ($1.1*10^{12}$ vg/per mouse), respectively. Four weeks after injection, the mice were euthanized and their tissues were harvested. To obtain obese mice, 8-week-old male C57BL/6 mice were fed a HFD for 16 weeks. Both ob/ob and HFD-induced obese mice were intraperitoneally injected with 3 mg/kg GCN2iB every other day. After 6 weeks, mice were euthanized for subsequent experiments.

4.2. Tissue processing and histological analyses

Mouse liver tissues were harvested rapidly, fixed, embedded, sectioned (5 μm) and then stained with H&E to assess hepatic steatosis. Frozen liver sections (4 μm) were stained with oil red O or DHE for 30 min to assess lipid accumulation and superoxide generation, respectively.

4.3. Measurement of serum and liver biochemical markers

Serum ALT, AST, TG, NEFA and insulin levels were measured with commercial kits. The OGTT was performed using an oral gavage of 2 g/kg glucose after overnight fasting [47]. The ITT was performed via intraperitoneal injection of 0.75 U/kg insulin after fasting for 4 h. At least 5 mice/group were used for each assay.

4.4. Cell culture

HepG2, L02 and 293T cells were obtained from the Cell Bank of the Institute of Biochemistry and Cell Biology (Shanghai, China). A murine liver cell line (NCTC 1469) was purchased from Procell Life Science & Technology Co., Ltd. (#CL-0407, Wuhan, China). Cells were grown in DMEM supplemented with 10% fetal bovine serum and 1% penicillin and streptomycin at 37 °C with 5% CO_2.

4.5. Recombinant adeno-associated virus serotype 8 gene therapy

A shRNA sequence targeting *Gcn2* (5′-GGTATACAATGCTTTGGAA-3′) or *Nrf2* (CCAAAGCTAGTATAGCAATAA) was constructed and inserted into the pAV-U6-GFP vector for viral packaging. Recombinant AAV8-GFP, AAV8-sh*Gcn2* and AAV8-sh*Nrf2* were produced by Vigene Biosciences. Inc. (Shandong, China).

4.6. RNA-sequencing

Briefly, RNA was extracted from the livers using TRIzol reagent followed by purification with DNase I treatment and rRNA removal. The RNA samples were then subjected to library construction and RNA sequencing using a BGISEQ500 platform (BGI-Shenzhen, China). SOAPnuke and Trimmomatic software [48] were used to treat the raw data. After mapping the clean reads to the reference genome (Mus_musculus, GCF_000001635.25_GRCm38.p5), the gene expression level and the DEGs between the two groups was obtained with RESM software [49] and DEGseq [50], respectively. The identified DEGs for each pair were then mapped to terms in the KEGG database (http://www.genome.jp/kegg/pathway.html), and a q-value ≤ 0.05 was considered to indicate significant enrichment.

4.7. Untargeted metabolomics analysis

Briefly, 25 mg of liver tissue was mixed with 500 μL of extract solution [acetonitrile: methanol: water (2: 2: 1) with isotopically labeled internal standard mixture]. The samples were homogenized at 35 Hz for 4 min and sonicated for 5 min at 0 °C. After 3 cycles of homogenization and sonication, the samples were incubated for 1 h at −40 °C and centrifuged at 12000 rpm for 15 min at 4 °C. The resulting supernatant was transferred to a fresh glass vial for analysis.

LC-MS/MS analyses were performed on an UHPLC system (Vanquish, Thermo Fisher Scientific) coupled to a Q Exactive HFX mass spectrometer (Orbitrap MS, Thermo), which acquired MS/MS spectra in information-dependent acquisition (IDA) mode using the acquisition software (Xcalibur, Thermo). Chromatographic separation was achieved on an UPLC BEH amide column (2.1 mm × 100 mm, 1.7 μm) maintained at 4 °C. Ammonium acetate (25 mmol/L) and ammonia hydroxide (25 mmol/L) in water (pH = 9.75) were used as mobile phase A, and acetonitrile was used as mobile phase B. The electrospray ionization (ESI) source conditions were set as follows: sheath gas flow rate of 30 Arb, Aux gas flow rate of 25 Arb, capillary temperature of 350 °C, full MS resolution of 60000, MS/MS resolution of 7500, collision energy of 10/30/60 in NCE mode, and spray voltage of 3.6 kV (positive) or −3.2 kV (negative).

4.8. Data and statistical analyses

The number of samples or animals is specified in the caption for each experiment. Data are expressed as the mean ± standard error. Statistical significance was defined as $p < 0.05$. Student's t-test or one-way analysis of variance (ANOVA) followed by Fisher's least significant difference test or the Kruskal-Wallis nonparametric test followed by Dunn's test was used to test differences in each variable among the treatment groups with GraphPad Prism 7 (GraphPad Software Inc., CA, USA).

Declaration of competing interest

The authors declare that they have no known competing financial interests or personal relationships that could have appeared to influence the work reported in this paper.

Acknowledgments

This study was supported by grants from National Natural Science Foundation of China (82070250) and the Fundamental Research Funds for the Central Universities.

Appendix A. Supplementary data

Supplementary data to this article can be found online at https://doi.org/10.1016/j.redox.2021.102224.

References

[1] E.M. Brunt, V.W. Wong, V. Nobili, C.P. Day, S. Sookoian, J.J. Maher, E. Bugianesi, C.B. Sirlin, B.A. Neuschwander-Tetri, M.E. Rinella, Nonalcoholic fatty liver disease, Nat. Rev. Dis. Prim. 1 (2015), 15080.
[2] V. Zambo, L. Simon-Szabo, P. Szelenyi, E. Kereszturi, G. Banhegyi, M. Csala, Lipotoxicity in the liver, World J. Hepatol. 5 (10) (2013) 550–557.
[3] M.G. Neuman, S.W. French, B.A. French, H.K. Seitz, L.B. Cohen, S. Mueller, N. A. Osna, K.K. Kharbanda, D. Seth, A. Bautista, K.J. Thompson, I.H. McKillop, I. A. Kirpich, C.J. McClain, R. Bataller, R.M. Nanau, M. Voiculescu, M. Opris, H. Shen, B. Tillman, J. Li, H. Liu, P.G. Thomes, M. Ganesan, S. Malnick, Alcoholic and non-alcoholic steatohepatitis, Exp. Mol. Pathol. 97 (3) (2014) 492–510.
[4] K. Hino, S. Nishina, K. Sasaki, Y. Hara, Mitochondrial damage and iron metabolic dysregulation in hepatitis C virus infection, Free Radical Biol. Med. 133 (2019) 193–199.
[5] P.J. Trivedi, D.H. Adams, Gut-liver immunity, J. Hepatol. 64 (5) (2016) 1187–1189.
[6] E. Crosas-Molist, I. Fabregat, Role of NADPH oxidases in the redox biology of liver fibrosis, Redox Biol. 6 (2015) 106–111.
[7] S. Milic, D. Lulic, D. Stimac, Non-alcoholic fatty liver disease and obesity: biochemical, metabolic and clinical presentations, World J. Gastroenterol. 20 (28) (2014) 9330–9337.
[8] H. Cichoz-Lach, A. Michalak, Oxidative stress as a crucial factor in liver diseases, World J. Gastroenterol. 20 (25) (2014) 8082–8091.
[9] A. Kobayashi, M.I. Kang, H. Okawa, M. Ohtsuji, Y. Zenke, T. Chiba, K. Igarashi, M. Yamamoto, Oxidative stress sensor Keap1 functions as an adaptor for Cul3-based E3 ligase to regulate proteasomal degradation of Nrf2, Mol. Cell. Biol. 24 (16) (2004) 7130–7139.
[10] K. Itoh, N. Wakabayashi, Y. Katoh, T. Ishii, K. Igarashi, J.D. Engel, M. Yamamoto, Keap1 represses nuclear activation of antioxidant responsive elements by Nrf2 through binding to the amino-terminal Neh2 domain, Gene Dev. 13 (1) (1999) 76–86.
[11] W. Li, S. Yu, T. Liu, J.H. Kim, V. Blank, H. Li, A.N. Kong, Heterodimerization with small Maf proteins enhances nuclear retention of Nrf2 via masking the NESzip motif, Biochim. Biophys. Acta 1783 (10) (2008) 1847–1856.
[12] P.J. Meakin, S. Chowdhry, R.S. Sharma, F.B. Ashford, S.V. Walsh, R.J. McCrimmon, A.T. Dinkova-Kostova, J.F. Dillon, J.D. Hayes, M.L. Ashford, Susceptibility of Nrf2-null mice to steatohepatitis and cirrhosis upon consumption of a high-fat diet is associated with oxidative stress, perturbation of the unfolded protein response, and disturbance in the expression of metabolic enzymes but not with insulin resistance, Mol. Cell. Biol. 34 (17) (2014) 3305–3320.
[13] S. Chowdhry, M.H. Nazmy, P.J. Meakin, A.T. Dinkova-Kostova, S.V. Walsh, T. Tsujita, J.F. Dillon, M.L. Ashford, J.D. Hayes, Loss of Nrf2 markedly exacerbates nonalcoholic steatohepatitis, Free Radical Biol. Med. 48 (2) (2010) 357–371.
[14] Y.K. Zhang, R.L. Yeager, Y. Tanaka, C.D. Klaassen, Enhanced expression of Nrf2 in mice attenuates the fatty liver produced by a methionine- and choline-deficient diet, Toxicol. Appl. Pharmacol. 245 (3) (2010) 326–334.
[15] D.H. Lee, D.H. Han, K.T. Nam, J.S. Park, S.H. Kim, M. Lee, G. Kim, B.S. Min, B. S. Cha, Y.S. Lee, S.H. Sung, H. Jeong, H.W. Ji, M.J. Lee, J.S. Lee, H.Y. Lee, Y. Chun, J. Kim, M. Komatsu, Y.H. Lee, S.H. Bae, Ezetimibe, an NPC1L1 inhibitor, is a potent Nrf2 activator that protects mice from diet-induced nonalcoholic steatohepatitis, Free Radical Biol. Med. 99 (2016) 520–532.
[16] R. Sood, A.C. Porter, D.A. Olsen, D.R. Cavener, R.C. Wek, A mammalian homologue of GCN2 protein kinase important for translational control by phosphorylation of eukaryotic initiation factor-2alpha, Genetics 154 (2) (2000) 787–801.
[17] H.P. Harding, I. Novoa, Y. Zhang, H. Zeng, R. Wek, M. Schapira, D. Ron, Regulated translation initiation controls stress-induced gene expression in mammalian cells, Mol. Cell 6 (5) (2000) 1099–1108.
[18] C. Chaveroux, S. Lambert-Langlais, L. Parry, V. Carraro, C. Jousse, A.C. Maurin, A. Bruhat, G. Marceau, V. Sapin, J. Averous, P. Fafournoux, Identification of GCN2 as new redox regulator for oxidative stress prevention in vivo, Biochem. Biophys. Res. Commun. 415 (1) (2011) 120–124.
[19] G.J. Wilson, B.A. Lennox, P. She, E.T. Mirek, R.J. Al Baghdadi, M.E. Fusakio, J. L. Dixon, G.C. Henderson, R.C. Wek, T.G. Anthony, GCN2 is required to increase fibroblast growth factor 21 and maintain hepatic triglyceride homeostasis during asparaginase treatment, American journal of physiology, Endocrinol. Metabol. 308 (4) (2015) E283–E293.
[20] S. Liu, J. Yuan, W. Yue, Y. Bi, X. Shen, J. Gao, X. Xu, Z. Lu, GCN2 deficiency protects against high fat diet induced hepatic steatosis and insulin resistance in mice, Biochimica et biophysica acta, Mol. Basis Dis. 1864 (10) (2018) 3257–3267.
[21] X. Zhang, N. He, Y. Xing, Y. Lu, Knockdown of GCN2 inhibits high glucose-induced oxidative stress and apoptosis in retinal pigment epithelial cells, Clin. Exp. Pharmacol. Physiol. 47 (4) (2020) 591–598.
[22] K. Tsuchida, T. Tsujita, M. Hayashi, A. Ojima, N. Keleku-Lukwete, F. Katsuoka, A. Otsuki, H. Kikuchi, Y. Oshima, M. Suzuki, M. Yamamoto, Halofuginone enhances the chemo-sensitivity of cancer cells by suppressing NRF2 accumulation, Free Radical Biol. Med. 103 (2017) 236–247.
[23] T.L. Keller, D. Zocco, M.S. Sundrud, M. Hendrick, M. Edenius, J. Yum, Y.J. Kim, H. K. Lee, J.F. Cortese, D.F. Wirth, J.D. Dignam, A. Rao, C.Y. Yeo, R. Mazitschek, M. Whitman, Halofuginone and other febrifugine derivatives inhibit prolyl-tRNA synthetase, Nat. Chem. Biol. 8 (3) (2012) 311–317.
[24] G.R. Masson, Towards a model of GCN2 activation, Biochem. Soc. Trans. 47 (5) (2019) 1481–1488.
[25] P. Rada, A.I. Rojo, N. Evrard-Todeschi, N.G. Innamorato, A. Cotte, T. Jaworski, J. C. Tobón-Velasco, H. Devijver, M.F. García-Mayoral, F. Van Leuven, J.D. Hayes, G. Bertho, A. Cuadrado, Structural and functional characterization of Nrf2 degradation by the glycogen synthase kinase 3/β-TrCP axis, Mol. Cell. Biol. 32 (17) (2012) 3486–3499.
[26] P. Rada, A.I. Rojo, S. Chowdhry, M. McMahon, J.D. Hayes, A. Cuadrado, SCF/{beta}-TrCP promotes glycogen synthase kinase 3-dependent degradation of the Nrf2 transcription factor in a Keap1-independent manner, Mol. Cell. Biol. 31 (6) (2011) 1121–1133.
[27] S. Chowdhry, Y. Zhang, M. McMahon, C. Sutherland, A. Cuadrado, J.D. Hayes, Nrf2 is controlled by two distinct β-TrCP recognition motifs in its Neh6 domain, one of which can be modulated by GSK-3 activity, Oncogene 32 (32) (2013) 3765–3781.
[28] J. Ye, W. Palm, M. Peng, B. King, T. Lindsten, M.O. Li, C. Koumenis, C. B. Thompson, GCN2 sustains mTORC1 suppression upon amino acid deprivation by inducing Sestrin2, Gene Dev. 29 (22) (2015) 2331–2336.
[29] O. Kaidanovich-Beilin, J.R. Woodgett, GSK-3: functional insights from cell biology and animal models, Front. Mol. Neurosci. 4 (2011) 40.
[30] A. Singh, S. Venkannagari, K.H. Oh, Y.Q. Zhang, J.M. Rohde, L. Liu, S. Nimmagadda, K. Sudini, K.R. Brimacombe, S. Gajghate, J. Ma, A. Wang, X. Xu, S. A. Shahane, M. Xia, J. Woo, G.A. Mensah, Z. Wang, M. Ferrer, E. Gabrielson, Z. Li, F. Rastinejad, M. Shen, M.B. Boxer, S. Biswal, Small molecule inhibitor of NRF2 selectively intervenes therapeutic resistance in KEAP1-deficient NSCLC tumors, ACS Chem. Biol. 11 (11) (2016) 3214–3225.
[31] P. Falcón, M. Escandón, Á. Brito, S. Matus, Nutrient Sensing and Redox Balance: GCN2 as a New Integrator in Aging, Oxidative Medicine and Cellular Longevity 2019, 2019, p. 5730532.
[32] Y. Wang, T. Lei, J. Yuan, Y. Wu, X. Shen, J. Gao, W. Feng, Z. Lu, GCN2 deficiency ameliorates doxorubicin-induced cardiotoxicity by decreasing cardiomyocyte apoptosis and myocardial oxidative stress, Redox Biol. 17 (2018) 25–34.
[33] M. Komatsu, H. Kurokawa, S. Waguri, K. Taguchi, A. Kobayashi, Y. Ichimura, Y. S. Sou, I. Ueno, A. Sakamoto, K.I. Tong, M. Kim, Y. Nishito, S. Iemura, T. Natsume, T. Ueno, E. Kominami, H. Motohashi, K. Tanaka, M. Yamamoto, The selective autophagy substrate p62 activates the stress responsive transcription factor Nrf2 through inactivation of Keap1, Nat. Cell Biol. 12 (3) (2010) 213–223.
[34] W. Chen, Z. Sun, X.J. Wang, T. Jiang, Z. Huang, D. Fang, D.D. Zhang, Direct interaction between Nrf2 and p21(Cip1/WAF1) upregulates the Nrf2-mediated antioxidant response, Mol. Cell 34 (6) (2009) 663–673.
[35] D.A. Cross, D.R. Alessi, P. Cohen, M. Andjelkovich, B.A. Hemmings, Inhibition of glycogen synthase kinase-3 by insulin mediated by protein kinase B, Nature 378 (6559) (1995) 785–789.
[36] S. Lageix, J. Zhang, S. Rothenburg, A.G. Hinnebusch, Interaction between the tRNA-binding and C-terminal domains of Yeast Gcn2 regulates kinase activity in vivo, PLoS Genet. 11 (2) (2015), e1004991.
[37] S.A. Wek, S. Zhu, R.C. Wek, The histidyl-tRNA synthetase-related sequence in the eIF-2 alpha protein kinase GCN2 interacts with tRNA and is required for activation in response to starvation for different amino acids, Mol. Cell. Biol. 15 (8) (1995) 4497–4506.
[38] A.J. Inglis, G.R. Masson, S. Shao, O. Perisic, S.H. McLaughlin, R.S. Hegde, R. L. Williams, Activation of GCN2 by the ribosomal P-stalk, Proc. Natl. Acad. Sci. U.S. A. 116 (11) (2019) 4946–4954.
[39] M. Galicia-Moreno, S. Lucano-Landeros, H.C. Monroy-Ramirez, J. Silva-Gomez, J. Gutierrez-Cuevas, A. Santos, J. Armendariz-Borunda, Roles of Nrf2 in liver diseases: molecular, pharmacological, and epigenetic aspects, Antioxidants 9 (10) (2020) 980.
[40] C. Yan, Y. Zhang, X. Zhang, J. Aa, G. Wang, Y. Xie, Curcumin regulates endogenous and exogenous metabolism via Nrf2-FXR-LXR pathway in NAFLD mice, Biomed. Pharmacother. 105 (2018) 274–281.
[41] H. Yang, T. Yang, C. Heng, Y. Zhou, Z. Jiang, X. Qian, L. Du, S. Mao, X. Yin, Q. Lu, Quercetin improves nonalcoholic fatty liver by ameliorating inflammation, oxidative stress, and lipid metabolism in db/db mice, Phytother Res. : PTR 33 (12) (2019) 3140–3152.
[42] R.S. Sharma, D.J. Harrison, D. Kisielewski, D.M. Cassidy, A.D. McNeilly, J. R. Gallagher, S.V. Walsh, T. Honda, R.J. McCrimmon, A.T. Dinkova-Kostova, M.L. J. Ashford, J.F. Dillon, J.D. Hayes, Experimental nonalcoholic steatohepatitis and

liver fibrosis are ameliorated by pharmacologic activation of Nrf2 (NF-E2 p45-related factor 2), Cell. Mol. Gastroenterol. Hepatol. 5 (3) (2018) 367–398.
[43] Y. Honda, T. Kessoku, Y. Sumida, T. Kobayashi, T. Kato, Y. Ogawa, W. Tomeno, K. Imajo, K. Fujita, M. Yoneda, K. Kataoka, M. Taguri, T. Yamanaka, Y. Seko, S. Tanaka, S. Saito, M. Ono, S. Oeda, Y. Eguchi, W. Aoi, K. Sato, Y. Itoh, A. Nakajima, Efficacy of glutathione for the treatment of nonalcoholic fatty liver disease: an open-label, single-arm, multicenter, pilot study, BMC Gastroenterol. 17 (1) (2017) 96.
[44] D. Rajcic, A. Baumann, A. Hernández-Arriaga, A. Brandt, A. Nier, C.J. Jin, V. Sánchez, F. Jung, A. Camarinha-Silva, I. Bergheim, Citrulline supplementation attenuates the development of non-alcoholic steatohepatitis in female mice through mechanisms involving intestinal arginase, Redox Biol. 41 (2021), 101879.
[45] Z. Yao, G. Liang, Z.L. Lv, L.C. Lan, F.L. Zhu, Q. Tang, L. Huang, X.Q. Chen, M. X. Yang, Q.W. Shan, Taurine reduces liver damage in non-alcoholic fatty liver disease model in rats by down-regulating IL-9 and tumor growth factor TGF-β, Bull. Exp. Biol. Med. 171 (5) (2021) 638–643.
[46] D.H. Munn, M.D. Sharma, B. Baban, H.P. Harding, Y. Zhang, D. Ron, A.L. Mellor, GCN2 kinase in T cells mediates proliferative arrest and anergy induction in response to indoleamine 2,3-dioxygenase, Immunity 22 (5) (2005) 633–642.
[47] S. Andrikopoulos, A.R. Blair, N. Deluca, B.C. Fam, J. Proietto, Evaluating the glucose tolerance test in mice, Am. J. Physiol. Endocrinol. Metabol. 295 (6) (2008) E1323–E1332.
[48] A.M. Bolger, M. Lohse, B. Usadel, Trimmomatic: a flexible trimmer for Illumina sequence data, Bioinformatics (Oxford, England) 30 (15) (2014) 2114–2120.
[49] B. Li, C.N. Dewey, RSEM: accurate transcript quantification from RNA-Seq data with or without a reference genome, BMC Bioinf. 12 (2011) 323.
[50] L. Wang, Z. Feng, X. Wang, X. Wang, X. Zhang, DEGseq: an R package for identifying differentially expressed genes from RNA-seq data, Bioinformatics (Oxf, Engl.) 26 (1) (2010) 136–138.

Abbreviations

3′-NT: 3′-nitrotyrosine
4-HNE: 4-hydroxynonenal
AAV8: recombinant adeno-associated virus serotype 8
ALT: alanine aminotransferase
AST: aspartate aminotransferase
ARE: antioxidant response element
β-TrCP: β-transducin repeat-containing protein
CHX: cycloheximide
Co-IP: coimmunoprecipitation
DHE: dihydroethidium
eIF2α: eukaryotic translation initiation factor 2 alpha
GCN2: general control nonderepressible 2
GFP: green fluorescent protein
GSK3-β: glycogen synthase kinase-3β
HF: halofuginone
HFD: high-fat diet
HO-1: heme oxygenase-1
ITT: insulin tolerance test
Keap1: Kelch-like ECH-associated protein 1
NAFLD: nonalcoholic fatty liver disease
NASH: nonalcoholic steatohepatitis
NEFA: nonesterified fatty acid
NQO1: quinone oxidoreductase-1
NRF2: nuclear factor erythroid 2-related factor 2
OGTT: oral glucose tolerance test
qRT-PCR: quantitative real-time polymerase chain reaction
ROS: reactive oxygen species
sgRNA: single guide RNA
tBHQ: tertiary butylhydroquinone
TG: triglyceride
TGF-β: transforming growth factor beta
TNFα: tumor necrosis factor alpha